PERGAMON

Available online at www.sciencedirect.com
SCIENCE DIRECT®

Solid State Communications 127 (2003) 89–98

solid state communications

www.elsevier.com/locate/ssc

Exciton condensation in coupled quantum wells

L.V. Butov[a,b,*]

[a]*Materials Sciences Division, E. O. Lawrence Berkeley National Laboratory, Berkeley, CA 94720, USA*
[b]*Institute of Solid State Physics, Russian Academy of Sciences, Chernogolovka 142432, Russian Federation*

Received 17 March 2003

Abstract

Bound electron–hole pairs—excitons—are Bose particles with small mass. Exciton Bose–Einstein condensation is expected to occur at a few degrees Kelvin—a temperature many orders of magnitude higher than for atoms. Experimentally, an exciton temperature well below 1 K is achieved in coupled quantum well (CQW) semiconductor nanostructures. In this contribution, we review briefly experiments that signal exciton condensation in CQWs: a strong enhancement of the indirect exciton mobility consistent with the onset of exciton superfluidity, a strong enhancement of the radiative decay rate of the indirect excitons consistent with exciton condensate superradiance, strong fluctuations of the indirect exciton emission consistent with critical fluctuations near the phase transition, and a strong enhancement of the exciton scattering rate with increasing concentration of the indirect excitons revealing bosonic stimulation of exciton scattering. Novel experiments with exciton condensation in potential traps, pattern formation in exciton system and macroscopically ordered exciton state will also be reviewed briefly.

PACS: 71.35. − y; 73.20.Dx; 78.55

Keywords: A. Quantum wells; D. Exciton; D. Condensation

1. Introduction

More than three decades ago Keldysh and Kozlov [1] showed that in the dilute limit, $na_B^D \ll 1$ (a_B is the exciton Bohr radius, n the exciton density, and D the dimensionality), excitons are weakly interacting Bose particles and are expected to undergo Bose–Einstein condensation (BEC). Because the exciton mass, M, is small—even smaller than the free electron mass—exciton condensation should occur at temperatures of about 1 K, several orders of magnitude higher than for atoms. Discovery of atom BEC is reviewed in Refs. [2,3].

In spite of the relatively high T_c it is experimentally challenging to lower the temperature of a high-density exciton gas enough to reach exciton condensation. Cooling semiconductor lattices well below 1 K is routinely achieved with He-refrigerators. Nevertheless, the exciton temperature, T_X, is determined by the ratio of the exciton energy relaxation and recombination rates and can considerably exceed that of the lattice. In order to create a cold exciton gas with T_X close to the lattice temperature, the exciton lifetime should considerably accede the exciton energy relaxation time.

Over the last two decades the experimental efforts to observe exciton BEC in bulk semiconductors dealt mainly with bulk Cu_2O [4,5], a material whose ground exciton state is optically dipole-inactive and has, therefore, a low radiative recombination rate. The conditions necessary for realization of BEC in Cu_2O appeared to be experimentally accessible: $T_c^{3D} = 0.527(2\pi\hbar^2/M)(n/g)^{2/3}$ (g is the spin degeneracy of the exciton state) would reach $\simeq 2.3$ K at exciton density $n = 10^{17}$ cm^{-3}. However, another, competitive density-dependent process turns on at high n : the exciton Auger recombination rate, $\propto n$, which increases faster than T_c with increasing n. Recent measurements indicate that the Auger recombination rate in Cu_2O is about two orders of magnitude higher than was assumed before

* Address: Materials Sciences Division, E. O. Lawrence Berkeley National Laboratory, Berkeley, CA 94720, USA.
E-mail address: lvbutov@lbl.gov (L.V. Butov).

0038-1098/03/$ - see front matter © 2003 Elsevier Science Ltd. All rights reserved.
doi:10.1016/S0038-1098(03)00312-0

and, therefore, the exciton densities reached in the up-to-date experiments are far below that required to achieve a degenerate Bose-gas of excitons [6]. The history and present status of experimental searches for exciton BEC in semiconductor materials is beyond the scope of this short contribution and will be reviewed elsewhere.

Due to long lifetimes and high cooling rates indirect excitons in coupled quantum wells (CQWs) (Fig. 1(a) and (b)) form a unique system where a cold exciton gas with temperatures below critical temperature for exciton condensation can be created. The long lifetimes of indirect excitons originate from the spatial separation between the electron and hole layers [7], resulting in a radiative lifetime of indirect excitons in CQWs samples that is more than three orders of magnitude longer than that of direct excitons in single QWs. The cooling of hot photoexcited excitons down to the temperatures of the cold lattice, which occurs via emission of bulk LA phonons, is about three orders of magnitude faster for excitons in GaAs QWs than that in bulk GaAs. This is due to relaxation of the momentum conservation law in the direction perpendicular to the QW plane. Indeed, for quasi-2D systems the ground-state mode $E = 0$ couples to the continuum of the energy states $E \geq E_0$ rather than to the single energy state $E = E_0 = 2Mv_s^2$ (v_s is the sound velocity) as it occurs in bulk semiconductors [8] (Fig. 1(c)).

A few words about peculiarities of condensation in 2D systems: for infinite 2D systems BEC, i.e. the macroscopic occupation of one (lowest energy) state with the number of particles in the state comparable with the total number of particles in the system, is possible only at $T = 0$. At finite temperatures, only condensation into a superfluid state with the mean-field transition temperature $T_c \approx 4\pi\hbar^2 n/[2m \ln \ln (1/na^2)]$ is possible in the weakly interacting Bose gas in two dimensions (n is the density, m is the boson mass, and a is the range of interaction) [9,10]. Below T_c the small momentum particles contribute to a so called quasicondensate, which results in the appearance of superfluidity [9,10]. Note that above the Kosterlitz–Thouless critical temperature, at $T_{KT} < T \lesssim T_c$, the superfluidity is local, and a macroscopic superfluid density abruptly appears at $T = T_{KT}$ [11]. For a finite 2D system with an area S, the critical temperature for BEC is nonzero: $T_{cS} = 2\pi\hbar^2 n/[mg \ln(nS/g)]$ [12], and reduces logarithmically with the increase of the system area (similarly, the critical temperature for BEC in 2D harmonic potential trap $T_c = (\sqrt{6}/\pi)\hbar\omega\sqrt{N/g}$ is finite for finite $\hbar\omega$—the quantization energy, N is the number of excitons in the trap). The difference between the quasicondensate (macroscopic occupation of the low momentum/energy states) and Bose–Einstein condensate (macroscopic occupation of one state) is not essential for most experiments [9] and unambiguous distinguishing between them in experiments is hard (if possible); therefore we will not distinguish between them discussing exciton condensation in the paper.

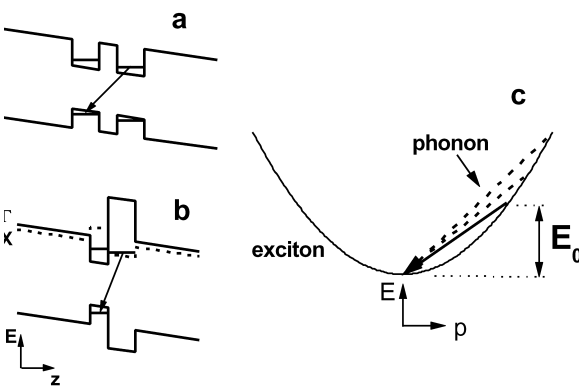

Fig. 1. Energy band diagram of GaAs/AlGaAs (a) and AlAs/GaAs (b) CQWs. The indirect transition is indicated by the arrow. (c) Energy diagram for the LA-phonon-assisted relaxation for bulk excitons (solid arrow) and for QW excitons (solid and dashed arrows).

Before starting the short review of experimental data on exciton condensation in CQWs, we mention briefly some specific properties of the indirect excitons. An intrinsic property of any QW systems is in-plane disorder potential, which is caused by interface and alloy fluctuations, defects and impurities, and is unavoidable in any QW sample. High quality samples are characterized by small amplitude and large length scale of the random potential. This is revealed by a small linewidth of exciton PL. Moderate in-plane random potential improves conditions for the exciton condensation in local potential energy minima because of the confinement effects and the enhanced local density driven by the exciton drift toward the bottom of the traps [13–15]. On a large scale, exciton condensate in a random potential is analogous to the 'Bose-glass' phase, or to a random Josephson-junction array in superconductors (see Ref. [13] and references therein). With the increase of the potential fluctuations the sizes of the condensate lakes (as well as the correlations between the lakes) are reduced, and at large random potential exciton condensate disappears. Therefore, in order to observe exciton condensate, high quality samples with small potential fluctuations are required. No condensation effects are observed in CQW samples with a large random potential. The experiments reviewed in the following sections were performed on the high quality CQW samples characterized by the narrowest PL linewidths.

In the absence of in-plane forces, an indirect exciton is a dipole oriented perpendicular to the QW plane. An interaction between such dipoles is repulsive. The repulsive interaction between the indirect excitons is advantageous for exciton condensation: it stabilizes exciton state against formation of metallic electron–hole droplets [16,17] and results in effective screening of an in-plane disorder potential [18]. Experimentally, the repulsive interaction is revealed by the enhancement of the exciton energy with increasing density [19–21]. We will return to the issue of the interaction between the indirect excitons in Section 5.

The electric field in the z direction is controlled by external gate voltage V_g. At low V_g (direct regime), the spatially direct exciton is the lowest energy state, while at high V_g (indirect regime) the indirect exciton composed of electron and hole in different layers is the lowest energy state. The transition from the direct to indirect regimes is determined by the ratio between the one-particle symmetric–antisymmetric splittings and the exciton binding energies. For a given CQW sample, this ratio and, in turn, the direct-to-indirect crossover can be controlled by magnetic fields [21–23]. The existence of both direct and indirect regimes in one and the same sample allows verifying an existence of condensation effects for direct and indirect excitons. In all the experiments reviewed below, only longlife indirect excitons, which are cold, exhibit the condensation effects; no condensation effects are observed for direct excitons, which cannot thermalize down to low temperatures within their short lifetime.

We note that a review of experiments on indirect excitons in CQWs made by other research groups (see, e.g. Refs. [24–27]) is beyond the scope of this short contribution and will be presented elsewhere.

2. Anomalous transport and luminescence of indirect excitons in AlAs/GaAs CQWs as evidence for exciton superfluidity, superradiance of the exciton condensate, and fluctuations near the phase transition

Lerner and Lozovik and Kuramoto and Horie showed that the critical conditions for exciton condensation in QWs can be drastically improved by high magnetic field perpendicular to the well plane [28,29]. The effect of the magnetic field can be understood qualitatively in terms of an attraction in momentum space due to the coupling between the exciton center-of-mass motion and internal structure. This coupling modifies the nature of exciton condensation: at $B = 0$ exciton condensation is purely determined by the statistical distribution in momentum space of weakly interacting bosons (i.e. excitons) [1], while in the high magnetic field regime, due to the coupling, the e–h Coulomb attraction forces the excitons to the low-momentum states, and, therefore, the mean-field critical temperature T_c at which the quasicondensate appears [9,10] in the high magnetic field limit is determined (within the mean-field approximation valid at not very low LL filling factors) by the e–h pairing [28,29] similar to the case of the excitonic insulator [30] or Cooper pairs. According to the theory of Refs. [28,29], T_c in high magnetic fields is much higher than T_c at $B = 0$ (see for example Fig. 1 of Ref. [13]). Note that a magnetic field could increase the quantum degeneracy of a 2D exciton gas and improve the critical conditions for the exciton condensation only for the systems with a small separation between electron and hole layers, d, while for the systems with a large d the magnetic field effect is dominated by the exciton mass enhancement that reduces the quantum degeneracy of 2D exciton gas and T_c which are both $\propto 1/M$ [31]. Experimental studies of 2D exciton gas with a small separation between electron and hole layers were performed using AlAs/GaAs CQWs where d is about 3.5 nm (Fig. 1(b)).

Condensation of longlife interacting indirect excitons in CQWs should be accompanied by the appearance of exciton superfluidity [7]. The interaction results in the linear dispersion of the collective modes in the exciton system and, consequently, in fulfillment of the Landau criterion of superfluidity [7,28,29,32], while the problem of the order parameter phase fixation [33,34] is removed due to the long lifetime of indirect excitons [7,35]. For measurements of the exciton transport, we have used a time-of-flight technique: the PL decay from an unmasked part of the sample was compared with the PL decay from a part of the sample, which was covered by a nontransparent NiCr mask, leaving an array of 4 μm wide stripes uncovered and separated from each other by 32 μm [13]. The PL decay for the masked part of the sample is more rapid compared to that for the unmasked part due to the exciton transport out of the window regions. The measurements of the exciton transport in AlAs/GaAs CQW's performed simultaneously with the PL decay measurements, have shown that the exciton nonradiative lifetime τ_{nr} ($\approx \tau$, the exciton lifetime, for the studied AlAs/GaAs CQW's with low quantum efficiency) is mainly determined by exciton transport to nonradiative recombination centers and is reduced (increased) with the increase (reduction) of the exciton mobility. Therefore, for these samples, the faster PL decay corresponds to more rapid exciton transport. A strong enhancement of the exciton mobility is observed at the expected conditions for the exciton condensation, i.e. at low temperatures and high magnetic fields (Fig. 2(b) and (d)), and cannot be explained in terms of single exciton transport. A possible explanation for this effect, the validity of which is argued in Ref. [13], is the onset of exciton superfluidity. Conversely, the increase of the exciton mobility with temperature and its reduction with magnetic field observed at high temperatures and/or low magnetic fields are typical for thermally activated single exciton transport in a random potential [36,37].

Besides the exciton superfluidity, another signature of the exciton condensation is the onset of exciton superradiance (macroscopic dipole), which can be detected as an increase of the exciton radiative decay rate [13,14]. The effect originates from an enhancement of the exciton coherent area, which is determined by the exciton localization length and the exciton scattering length for normal excitons [38] and by the condensate size for condensed excitons, see Ref. [13] for details. The increase of the exciton radiative decay rate at the exciton condensation refers to the excitons that are direct in $x-y$ momentum space. The indirect excitons in the AlAs/GaAs CQWs studied in Refs. [13,19,20] are of X_z type, i.e. they are direct in $x-y$ momentum space. The exciton radiative

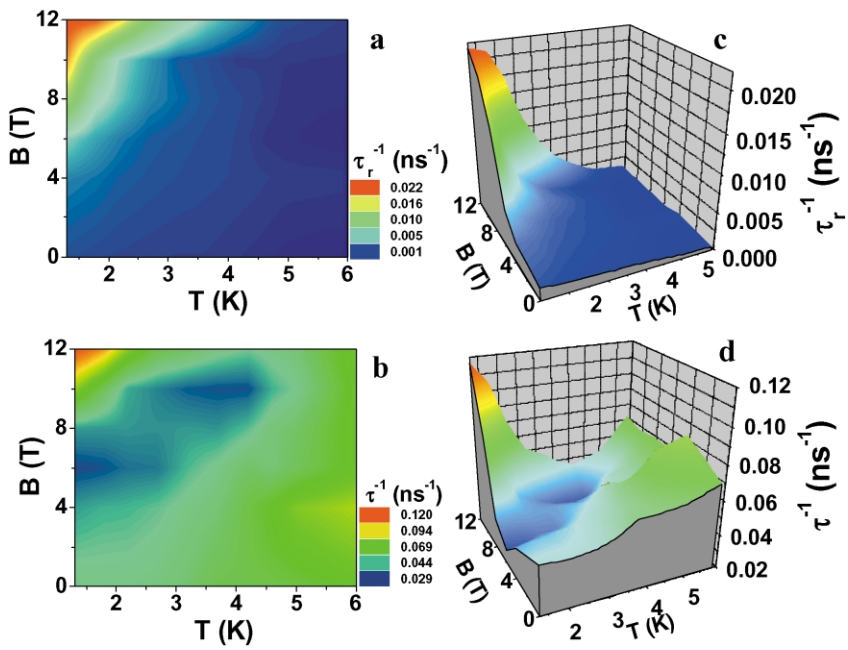

Fig. 2. Temperature and magnetic field dependences of the radiative decay rate τ_r^{-1} (a and c) and the initial decay rate τ^{-1} (b and d) of the indirect excitons in AlAs/GaAs CQW. The variations of τ^{-1} reflect the changes in exciton transport with the larger τ^{-1} corresponding to the faster exciton transport, see text.

decay rate τ_r^{-1} can be directly derived from the measured τ and the time-integrated exciton PL intensity I_{PL}. In the case of monoexponential PL decay $\tau_r^{-1} \approx (I_{PL}/I_D)\tau^{-1}$, where I_D is the integrated PL intensity in the direct regime measured at the same excitation (see Ref. [13] for details). A strong increase of τ_r^{-1} with reducing temperature and increasing magnetic field was observed [13]: the variation of τ_r^{-1} reaches about 60 times when going from the lower right corner to the upper left corner of the diagram plane (Fig. 2(a) and (c)). Because the strong increase of τ_r^{-1} is observed at the expected conditions for the exciton condensation, i.e. at low temperatures and high magnetic fields, and because this increase is expected for the exciton condensation and cannot be explained for normal uncondensed excitons, we believe that the observed huge increase of τ_r^{-1} corresponds to the exciton condensate superradiance, i.e. formation of a macroscopic dipole. Conversely, the small increase of τ_r^{-1} observed with increasing magnetic field at high temperatures, $\gtrsim 5$ K, corresponds to the shrinkage of the in-plane relative e–h wave function, while the small increase of τ_r^{-1} observed with reducing temperature at low magnetic fields, $B \lesssim 4$ T, corresponds to the gradual increase of $p < p_0$ state filling (Section 3) and the coherent area for normal uncondensed excitons. The anomalous rapid exciton transport and large τ_r^{-1} are observed in approximately the same range of parameters—at low temperatures and high magnetic fields (Fig. 2). They are strongly reduced with reducing excitation density W (while at low magnetic fields and high temperatures the exciton transport and τ_r^{-1} only weakly depend on W) [13]. This qualitatively corresponds to the expected disappearance of the exciton superfluidity and superradiance for the exciton condensate in a random potential [13].

A spectacular effect has been observed under cw photoexcitation in high magnetic fields, namely, a huge broad band noise in the integrated PL intensity of indirect excitons [19,20] (Fig. 3). The average variation of the integrated PL intensity is connected with variations of

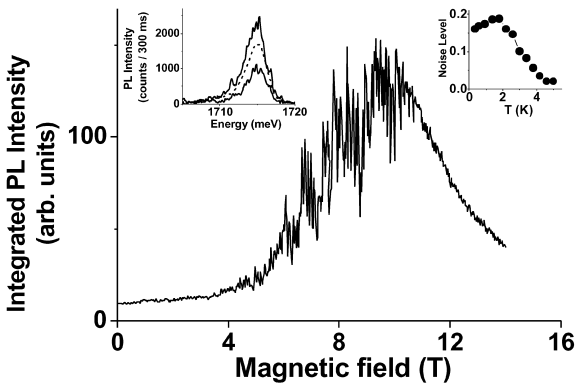

Fig. 3. Magnetic field dependence of the integrated PL intensity of the indirect excitons in AlAs/GaAs CQW at cw excitation at $T = 350$ mK. Right insert: temperature dependence of the noise level $\langle \delta I_{PL} \rangle / \langle I_{PL} \rangle$ at $B = 9$ T. Left insert: long time integrated indirect exciton PL spectrum and indirect exciton PL spectra integrated during 0.3 s in the noise regime.

radiative and nonradiative decay times of indirect excitons discussed above. The power spectrum of the anomalously large noise has a broadband spectrum. The noise is observed at low temperatures (Fig. 3). The spectral position of the PL line is practically constant during the intensity fluctuations (Fig. 3), which shows that the noise cannot be related to the fluctuations of the CQW potential profile in the z direction.

The appearance of the huge noise is strong evidence for the presence of coherence in the exciton system. The noise amplitude is known to be inversely proportional to the number of statistically independent entities in a system [39]. Large noise amplitudes therefore denote that only a small number of entities exist in the macroscopically large photoexcited region. The appearance of these macroscopic entities in the exciton system is consistent with the exciton condensation. A condensed lake can be considered as one macroscopic entity. Due to the high radiative decay rate of the exciton condensate, the PL signal of condensed excitons is much higher as compared to uncondensed ones. The formations and disappearances of condensate lakes therefore result in fluctuations of the total PL signal. Note that large fluctuations of the total PL signal are possible because of the small PL quantum efficiency of normal uncondensed indirect excitons, which can be strongly increased in the condensate lake sites at the exciton condensation. The noise is observed only on the left slope of the $I_{PL}(B)$ dependence (Fig. 3), i.e. the noise appears in the range of magnetic fields where τ_r^{-1} starts to increase, and disappears in the range of magnetic fields where τ_r^{-1} saturates and rapid exciton transport is observed. Therefore, the noise can be understood as the fluctuations near the phase transition connected with an unstability of the condensate lakes.

3. Bosonic stimulation of exciton scattering

The scattering rate of bosons to a state $\mathbf{p}$ is proportional to $(1+N_{\mathbf{p}})$, where $N_{\mathbf{p}}$ is the occupation number of the state $\mathbf{p}$. At high $N_{\mathbf{p}} \gtrsim 1$ the scattering process is stimulated by the presence of other identical bosons in the final state. The stimulated scattering is a signature of quantum degeneracy.

In this and the following sections, we review briefly experiments on excitons in the high quality GaAs/AlGaAs CQWs (Fig. 1(a)) where the radiative recombination is dominant. The PL kinetics of indirect excitons are shown in Fig. 4(a) [40]. At low excitations, after a rectangular excitation pulse is switched off, the PL intensity of indirect excitons decay nearly monoexponentially. In contrast, at high excitations, right after the excitation pulse is switched off the PL intensity first jumps up and starts to decay only in a few nanoseconds. For delocalized, in-plane free, quasi-2D excitons only the states with small center-of-mass momenta $|\mathbf{p}_\parallel| \le p_0 \simeq E_g\sqrt{\varepsilon_b}/c$ (E_g is the band gap and ε_b is the background dielectric constant) can decay radiatively by resonant emission of bulk photons [38] (Fig. 5(a)). Thus the

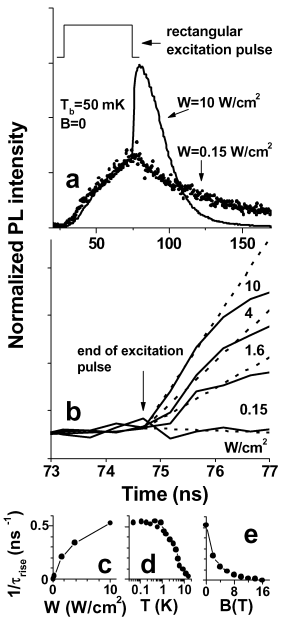

Fig. 4. (a) PL kinetics of indirect excitons in GaAs/AlGaAs CQW at high and low excitations W. (b) PL kinetics of indirect excitons near the end of the excitation pulse at different W. The rate $1/\tau_{rise}$ of the PL rise right after the end of the excitation pulse is presented in (c), (d), and (e) vs W at $T_b = 50$ mK and $B = 0$, bath temperature T_b at $W = 10$ W/cm^2 and $B = 0$, and magnetic field B at $W = 10$ W/cm^2 and $T_b = 50$ mK, respectively.

PL dynamics is determined by the occupation kinetics of the optically active low-energy states $E \le E_{p_0}$, the radiative zone ($E_{p_0}/k_B = p_0^2/2Mk_B \simeq 1.2$ K at $B = 0$). The LA-phonon-assisted relaxation of hot photoexcited indirect excitons into the optically active low-energy states results in a rise of the PL signal, while optical recombination of the low-energy indirect excitons results in a decay of the PL intensity. The end of the excitation pulse is accompanied by a sharp drop in the exciton temperature as caused by switching off the generation of hot indirect excitons and, as a result, the PL intensity and the occupation numbers $N_{E\le E_{P0}}$ of the optically active low-energy states abruptly rise within a few nanoseconds right after the trailing edge of the excitation pulse.

The measured PL kinetics is strongly nonlinear (Fig. 4(b) and (c)): the observed increase of τ_{rise}^{-1} with increasing exciton concentration (or W) proves that the scattering is stimulated by the final exciton state occupancy which, in turn, is high, $N_{\mathbf{p}\le\mathbf{p_0}} \gtrsim 1$. The observed decrease of τ_{rise}^{-1} with increasing temperature (Fig. 4(d)) results from a thermal reduction of the occupation of the low-energy exciton states $N_{\mathbf{p}\le\mathbf{p_0}}$. The observed decrease of τ_{rise}^{-1} in the presence of a magnetic field (Fig. 4(e)) is mainly caused by an increase of the magnetoexciton mass $M = M(B)$ [31,41]. Fig. 5(b) shows that the numerical simulations reproduce the observed PL dynamics [40]. According to the calculations plotted in Fig. 5(c), the end of the excitation pulse is indeed

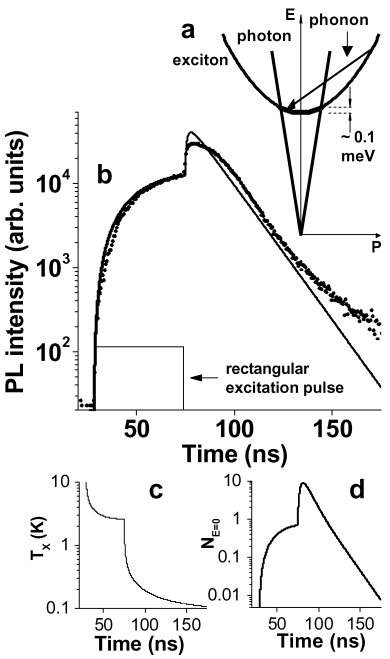

Fig. 5. (a) Energy diagram for the LA-phonon-assisted relaxation and optical decay of indirect excitons in GaAs/AlGaAs CQWs. The bold sector of the parabolic exciton dispersion indicates the radiative zone for indirect excitons. The calculated dynamics of (b) the PL intensity of indirect excitons $I_{PL}(t)$, (c) the effective exciton temperature $T_X(t)$, and (d) the ground-state occupation number $N_{E=0}(t)$ (lines). The parameters used in the numerical modelling refer to the experimental PL kinetics observed at $W = 10$ W/cm^2, $T_b = 50$ mK, $B = 0$ and shown in (b) by points.

accompanied by a sharp drop of T_X. According to Fig. 5(d), the PL jump after the pump pulse is accompanied by $N_{E=0} \gg 1$, i.e. a strongly degenerate Bose-gas of indirect excitons builds up.

4. Towards exciton condensation at potential traps

In this and the following section we review briefly recent experiments, which are currently in progress. The recent advances in BEC of atoms were made possible by exploiting the confinement of atomic gases within potential traps [2,3]. The conditions for BEC of indirect excitons are also significantly improved if they collected in a local minimum caused by an in-plane modulation of the potential. Then T_c increases because both of confinement effects and enhancement of the local density at the trap center that results from the drift of photoexcited excitons toward the bottom of the trap. As for atomic systems, excitons condense in real space in the lowest energy state at the bottom of the trap, which corresponds to the condensation in momentum space for infinite systems, i.e. to the BEC.

In-plane potential traps can be formed by lateral modulation of the electric field along $\vec{z}$ (E_z), by application of a local stress or of a local magnetic field. Besides this interesting approach intrinsic local minima of the in-plane potential are always present in any QW structure. These natural-traps are caused by random fluctuations of the interfaces, e.g. QW thickness and/or alloy disorder, or E_z. Such potential minima can host highly degenerate exciton systems and ultimately BEC [17]. There is a great variety of fluctuations in the random potential of any semiconductor heterostructure, e.g. width and depth. Therefore, among all the many traps present in a given sample, the exciton gas will by itself select those with optimal parameters for condensation. A signature of condensation of a degenerate exciton gas in such a trap is its strongly in-plane localized PL emission peaked at the bottom of the trap.

We have observed a huge local enhancement of the indirect exciton PL intensity that indicates the effective accumulation of excitons in specific natural-traps [15]. Under uniform excitation of a whole mesa using a defocused laser, the indirect exciton PL intensity at the center of a trap is about 30 times higher than that emitted from any other location on the mesa outside the trap. We have also explored the traps under inhomogeneous excitation using a smaller, 100×200 μm^2, laser spot that can be located anywhere on the mesa as far away from a trap as 400 μm. As seen in Fig. 6(a) and even in that case the indirect excitons are collected in the trap and the PL intensity from the trap is up to about six times higher than the PL intensity in the excitation spot. It is important to note that in the case of remote excitation the trap is filled by the cold excitons. In the remote excitation experiments the degenerate Bose-gas of indirect excitons builds up already outside the trap in the excitation spot, as revealed by the Bosonic stimulation of exciton scattering to the low-energy states (Section 3). The degree of quantum degeneracy is much higher for indirect excitons accumulated at the center of the trap. The diameter of the exciton cloud near the bottom of the potential trap reduces as the temperature is lowered while the peak intensity increases as shown in Fig. 6. This demonstrates that while at high temperatures the excitons are distributed over the high-energy states of the trap, at low temperatures the excitons condense at the bottom of the trap. Similar spatial shrinkage of atom clouds is characteristic of atomic BEC in the potential traps. We note, however, that the spatial shrinkage of the exciton cloud observed in the experiments of Ref. [15] does not allow to claim macroscopic occupation of one state, i.e. exciton BEC, in the traps.

5. Macroscopically ordered exciton phase

The initially photogenerated excitons are hot, however, they quickly cool down to the lattice temperature, $T_{lattice}$, via

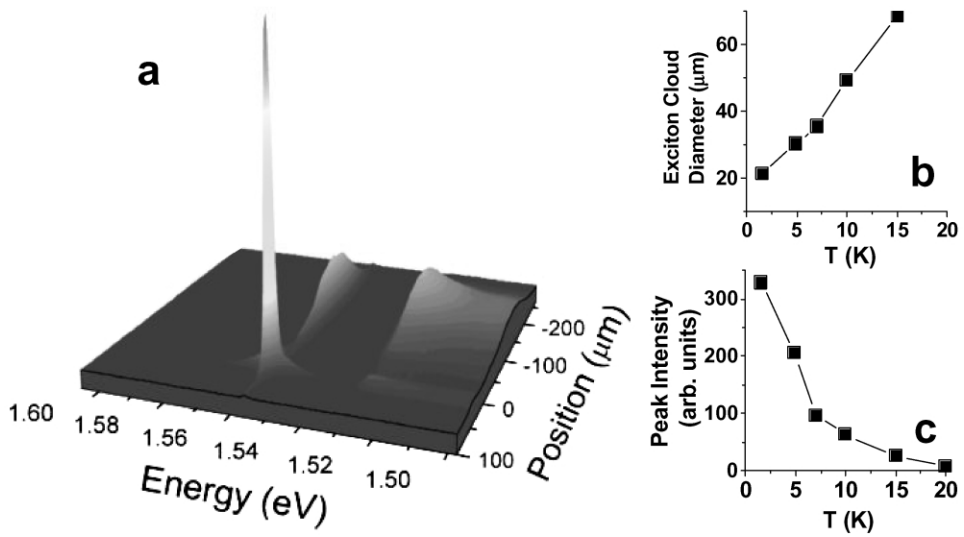

Fig. 6. (a) PL intensity vs energy and one of the in-plane coordinate at $T = 1.6$ K. The indirect exciton PL line is at ≈ 1.555 eV, the broad line below 1.53 eV comes from the bulk n^+-GaAs emission. The laser excitation is focused to $\sim 100 \times 200$ μm^2 spot about 170 μm away from the trap. The temperature dependence of (b) the diameter of the indirect exciton cloud and (c) their PL peak intensity.

phonon emission: e.g. the exciton temperature, T_X, can drop down to 400 mK in about 5 ns, that is the time much shorter than the indirect exciton lifetime (Fig. 5(c)). Therefore, there are two ways to overcome the obstacle of hot generation and study cold gases of indirect excitons with $T_X \approx T_{lattice}$: (1) use a separation in time and study the indirect excitons a few ns after the end of the photoexcitation pulses (Section 3) [40], (2) use a separation in space and study the indirect excitons beyond the photoexcitation spot. In the latter case, excitons can cool down to $T_{lattice}$ as they travel away from photoexcitation spot. In this section, we review briefly spatially and spectrally resolved PL experiments revealing a ring structure in the indirect exciton photoluminescence and a macroscopically ordered state of indirect excitons appearing in the ring the most remote from the excitation spot where the most cold exciton gas is formed [42].

At high excitation powers, P_{ex} the indirect exciton PL pattern is characterized by a ring structure: the laser excitation spot is surrounded by two concentric bright rings separated by an annular dark interring region (Fig. 7(a)). The rest of the sample outside the external ring is dark. The internal ring appears near the edge of the laser excitation spot, and the external ring can be remote from the excitation spot by more than 100 μm. Its radius increases with P_{ex}. The ring structure follows the laser excitation spot when it is moved over the whole sample area. When the temperature is increased the bright rings wash out and the PL profile approaches a monotonic bell-like shape [42]. We note that luminescence rings were observed also in other CQW materials [43].

The external ring is fragmented into circular-shape structures that form a periodic array over macroscopic lengths, up to ~ 1 mm (Fig. 8(a)). This is demonstrated in Fig. 8(d), which shows the nearly linear dependence of the fragment positions along the ring vs their number. The in-plane potential fluctuations are not strong enough to destroy the ordering (Fig. 8(d)). The fragments follow the external ring either when the excitation spot is moved over the sample area or when the ring radius varies with P_{ex}. Along the whole external ring, both in the peaks and the passes, the indirect exciton PL lines are spectrally narrow with the full width at half maximum ≈ 1.3 meV, considerably smaller than in the center of the excitation spot. The ring fragmentation into the periodic chain appears abruptly at low $T \lesssim 3$ K; this is quantified by the amplitude of the Fourier transform of the PL intensity variation along the ring (Fig. 8(e)).

The observed effects are discussed briefly below. The long lifetime of indirect excitons allows them to move far away from the excitation spot before they recombine. Under cw photoexcitation, there is a continuous flow of excitons out of the excitation spot owing to the exciton drift, diffusion, phonon wind, etc. The exciton diffusion originates directly from the exciton density gradient. The exciton drift also originates from the density gradient as the latter gives rise to the gradient of the indirect exciton potential energy because of the repulsive interaction (Fig. 7(b)). As the excitons travel away from the excitation spot, T_X decreases with increasing radial distance owing to the energy relaxation of the excitons. The reduction of T_X increases the radiative zone occupation (Section 3) and, therefore, increases the PL intensity; this is seen as the onset of the internal ring.

Travelling out of the potential energy ‘hill’ at the center of the excitation spot excitons acquire an average drift

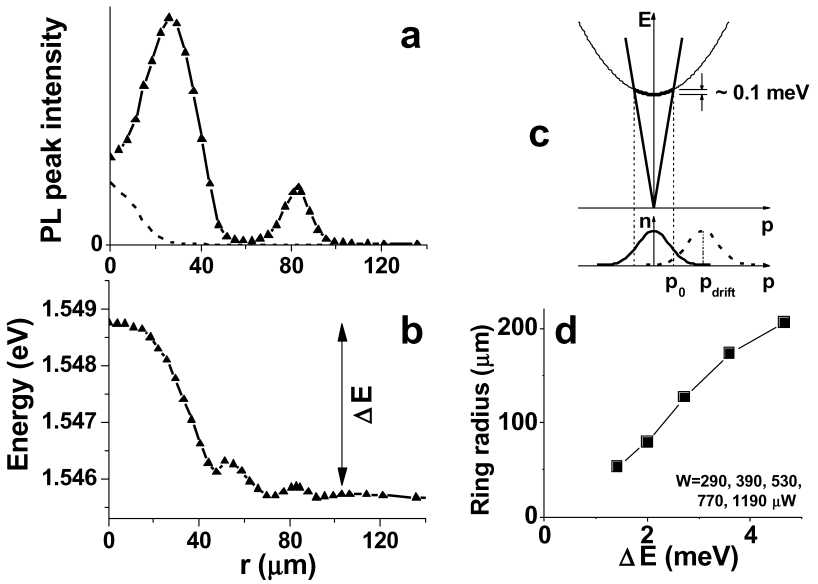

Fig. 7. (a) Peak intensity and (b) energy of the indirect exciton PL vs r, the distance from the excitation spot center, at $T = 1.8$ K, and the excitation power $P_{ex} = 390$ μW. The excitation spot profile is shown by the dashed line in (a). (c) Energy diagram for the exciton and photon dispersion, the bold sector of the exciton dispersion indicates the radiative zone. The lower part presents the schematic momentum distribution of excitons without (solid line) and with (dashed line) average drift velocity. The exciton radiative decay rate is proportional to the fraction of excitons in the radiative zone ($p < p_0$). (d) The external ring radius vs the height of the 'energy hill' shown in (b).

momentum, p_{drift}. As the height of the potential energy hill (Fig. 7(b)) is much larger than the kinetic energy at the radiative zone edge, $p_0^2/(2M) \sim 0.1$ meV, p_{drift} can exceed p_0. That means that the moving excitons become optically inactive (Fig. 7(c)). One aspect of this effect is that the optically inactive excitons move at speeds faster than the speed of sound. Far from the excitation spot the main driving force for exciton transport, the energy gradient, vanishes (Fig. 7(b)) and the excitons relax down to the lowest energy states. This results in the sharp enhancement

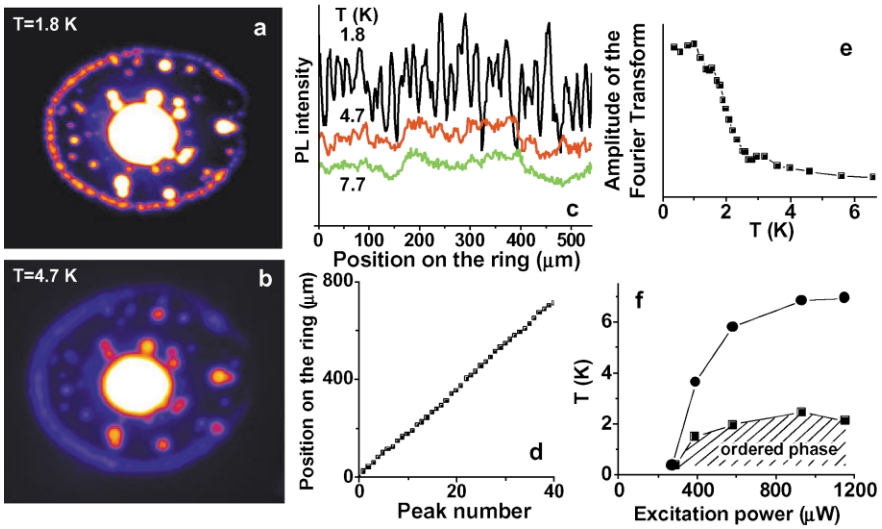

Fig. 8. Spatial pattern of the indirect exciton PL intensity at $T = 1.8$ (a) and 4.7 K (b) for $P_{ex} = 690$ μW. The area of view is 475×414 μm^2. (c) The corresponding variation of the indirect exciton PL intensity along the external ring at $T = 1.8$, 4.7, and 7.7 K. The dependence of the position of the indirect exciton PL intensity peaks along the external ring vs the peak number is nearly linear (d), showing that the fragments form a periodic chain. An amplitude of the Fourier transform at the period (e) shows that the macroscopically ordered phase appears abruptly at low temperatures. (f) The phase diagram for the exciton states in the external ring: the macroscopically ordered exciton phase is observed in the area terminated by squares (while the external ring itself appears with reducing temperature around dots).

of the radiative zone occupation and thus the PL intensity that contributes to the external ring. The external ring radius increases with the height of the potential energy hill (Fig. 7(d)). The exciton deceleration contributes also to the dense shell formation near the region where the excitons stop.

In the external ring the heating sources (such as hot photoexcited excitons in the excitation spot and the transformation of potential energy to kinetic when moving out of the energy hill in the dark interring region) vanish. It is the external ring where the most cold exciton gas is formed. The macroscopically ordered exciton state is formed in the external ring, i.e. in the most cold exciton gas. The existence of the periodic ordering shows that the exciton state formed in the external ring has a coherence on a macroscopic length scale. The phase diagram for the exciton states in the external ring is presented in Fig. 8(f). The macroscopically ordered exciton state is a new state that was not predicted, the understanding of its microscopic nature warrants future studies. We note that a spontaneous macroscopic ordering can occur both for quantum (e.g. soliton trains in atom BEC [44]) and classical (e.g. Taylor vortices [45]) systems. The macroscopic ordering is observed in the same temperature range as bosonic stimulation of exciton scattering (Section 3), below a few Kelvin. This implies that the macroscopic ordering could be an intrinsic property of a statistically degenerate Bose-gas of excitons, although just a coincidence of the parameters cannot be excluded.

The fragmentation of the exciton system, i.e. formation of higher density exciton clumps (that are qualitatively distinct from the metallic e–h droplets [46]), implies effective attractive interaction in the exciton system. Indeed, a repulsive interaction should suppress the fragmentation in exciton density, as it would be energetically unfavorable. In the experiments on atom BEC [44], the stripe of atom BEC was homogeneous in the case of repulsive interaction and, conversely, was fragmented to the periodic soliton train in the case of attractive interaction due to the modulational instability. Similarly, gravitational instability results in the fragmentation of gaseous slabs and filaments that is a step in formation of stars [47]. The fragmentation is natural in systems with an attractive interaction since it results in lowering the system energy.

In this paragraph, we discuss a possible scenarios for an attractive interaction for the indirect excitons in CQWs. For $r \gg d$, the interaction between oriented dipoles is $U = e^2d^2/(\varepsilon_b r^3)(1 - 3\cos^2\Theta)$, where r is the distance between the dipoles and Θ is the angle between $\mathbf{d}$ and $\mathbf{r}$. For the dipoles oriented perpendicular to the CQW plane the interaction is repulsive. However, the interaction would switch from repulsive to attractive for the dipoles tilted from the normal direction so that $1 - 3\cos^2\Theta < 0$. The titling of the dipoles causes the reduction of the exciton binding energy by δE_b that increases the system energy, while the switching from repulsive to attractive interaction between the dipoles lowers the system energy by δE_{int}. In the case if $\delta E_b > \delta E_{int}$ the tilting of the dipoles could be caused by an external in-plane electric field. Within this scenario, the interaction switches from repulsive to attractive when the external in-plane electric field exceeds the threshold, which is determined by $\delta E_b - \delta E_{int}$. A possible source for an in-plane electric field could be fluxes of photons and nonequilibrium phonons spreading mainly out of the excitation spot. Note that the use of off-resonant lasers to induce long-range dipole–dipole attractive interaction in atomic BEC was considered in Ref. [48,49]. In the case if $\delta E_b < \delta E_{int}$ the titling of the exciton dipoles is energetically favorable and, therefore, takes place spontaneously in the system leading to a new ground state.

6. Summary

In this contribution, we reviewed briefly the problem of exciton condensation in CQW semiconductor nanostructures where a cold exciton gas with temperatures below critical temperature for exciton condensation can be created. We reviewed experiments that signal exciton condensation in CQWs: a strong enhancement of the indirect exciton mobility consistent with the onset of exciton superfluidity, a strong enhancement of the radiative decay rate of the indirect excitons consistent with exciton condensate superradiance (i.e. macroscopic dipole), strong fluctuations of the indirect exciton emission consistent with critical fluctuations near the phase transition, and a strong enhancement of the exciton scattering rate with increasing concentration of the indirect excitons revealing bosonic stimulation of exciton scattering. Novel experiments with exciton condensation in potential traps, pattern formation in exciton system and macroscopically ordered exciton state were also reviewed briefly. The phase diagram for the macroscopically ordered exciton state was presented. A model aiming to develop an understanding of the macroscopically ordered exciton state was proposed.

Acknowledgements

The study of indirect excitons were performed in collaboration with G. Abstreiter, G. Böhm, K.L. Campman, D.S. Chemla, V.T. Dolgopolov, A.I. Filin, K. Eberl, A.C. Gossard, A. Imamoglu, A.L. Ivanov, P.B. Littlewood, Y.E. Lozovik, A.V. Mintsev, A.V. Petinova, A.A. Shashkin, G. Weimann, and A. Zrenner. We thank G.E.W. Bauer, A.B. Dzyubenko, N.A. Gippius, L.V. Keldysh, D.-H. Lee, and L.S. Levitov for valuable discussions.

References

[1] L.V. Keldysh, A.N. Kozlov, Zh. Eksp. Teor. Fiz. 54 (1968) 978 Sov. Phys. JETP 27, 521 (1968).

[2] E.A. Cornell, C.E. Wieman, Rev. Mod. Phys. 74 (2002) 875.
[3] W. Ketterle, Rev. Mod. Phys. 74 (2002) 1131.
[4] D.W. Snoke, J.P. Wolfe, A. Mysyrowicz, Phys. Rev. Lett. 59 (1987) 827.
[5] J.L. Lin, J.P. Wolfe, Phys. Rev. Lett. 71 (1993) 1222.
[6] K.E. O'Hara, L.O. Suilleabhain, J.P. Wolfe, Phys. Rev. B 60 (1999) 10565.
[7] Yu.E. Lozovik, V.I. Yudson, Zh. Eksp. Teor. Fiz. 71 (1976) 738 Sov. Phys. JETP 44, 389 (1976).
[8] A.L. Ivanov, P.B. Littlewood, H. Haug, Phys. Rev. B 59 (1999) 5032.
[9] V.N. Popov, Theor. Math. Phys. 11 (1972) 565. P.N. Brusov, V.N. Popov, Superfluidity and collective properties of quantum liquids Nauka Moscow (1988) Chapter 6.
[10] D.S. Fisher, P.C. Hohenberg, Phys. Rev. B 37 (1988) 4936.
[11] J.M. Kosterlitz, D.J. Thouless, J. Phys. C 6 (1973) 1181.
[12] W. Ketterle, N.J. van Drutten, Phys. Rev. A 54 (1996) 656.
[13] L.V. Butov, A.I. Filin, Phys. Rev. B 58 (1998) 1980.
[14] D.E. Nikonov and A. Imamoglu, quant-ph/9806003.
[15] L.V. Butov, C.W. Lai, A.L. Ivanov, A.C. Gossard, D.S. Chemla, Nature 417 (2002) 47.
[16] D. Yoshioka, A.H. MacDonald, J. Phys. Soc. Jpn 59 (1990) 4211.
[17] X. Zhu, P.B. Littlewood, M. Hybertsen, T. Rice, Phys. Rev. Lett. 74 (1995) 1633.
[18] A.L. Ivanov, Europhys. Lett. 59 (2002) 586.
[19] L.V. Butov, A. Zrenner, G. Böhm, G. Weimann, J. de Physique IV 3 (1993) 167.
[20] L.V. Butov, A. Zrenner, G. Abstreiter, G. Böhm, G. Weimann, Phys. Rev. Lett. 73 (1994) 304.
[21] L.V. Butov, A.A. Shashkin, V.T. Dolgopolov, K.L. Campman, A.C. Gossard, Phys. Rev. B 60 (1999) 8753.
[22] L.V. Butov, A. Zrenner, G. Abstreiter, A.V. Petinova, K. Eberl, Phys. Rev. B 52 (1995) 12153.
[23] A.B. Dzyubenko, A.L. Yablonskii, Phys. Rev. B 53 (1996) 16335.
[24] T. Fukuzawa, E.E. Mendez, J.M. Hong, Phys. Rev. Lett. 64 (1990) 3066.
[25] V. Negoita, D.W. Snoke, K. Eberl, Phys. Rev. B 60 (1999) 2661.
[26] A. Parlangeli, P.C.M. Christianen, J.C. Maan, I.V. Tokatly, C.B. Soerensen, P.E. Lindelof, Phys. Rev. B 62 (2000) 15323.
[27] A.V. Larionov, V.B. Timofeev, P.A. Ni, S.V. Dubonos, I. Hvam, K. Soerensen, Pis'ma ZhETF 75 (2002) 689 JETP Lett. 75, 570 (2002).
[28] Y. Kuramoto, C. Horie, Solid State Commun. 25 (1978) 713.
[29] I.V. Lerner, Yu.E. Lozovik, Zh. Eksp. Teor. Fiz. 78 (1978) 1167 Sov. Phys. JETP 51, 588 (1980).
[30] L.V. Keldysh, Yu.E. Kopaev, Zh. Eksp. Teor. Fiz. 6 (1964) 2791 Sov. Phys. Solid State 6, 6219 (1965).
[31] Yu.E. Lozovik, I.V. Ovchinnikov, S.Yu. Volkov, L.V. Butov, D.S. Chemla, Phys. Rev. B 65 (2002) 235304.
[32] D. Paquet, T.M. Rice, K. Ueda, Phys. Rev. B 32 (1985) 5208.
[33] W. Kohn, D. Sherrington, Rev. Mod. Phys. 42 (1970) 1.
[34] R.R. Guseinov, L.V. Keldysh, Zh. Eksp. Teor. Fiz. 63 (1972) 2255 Sov. Phys. JETP 36, 1193 (1973).
[35] Yu.E. Lozovik, V.I. Yudson, Pis'ma Zh. Eksp. Teor. Fiz. 25 (1977) 18 JETP Lett. 66, 355 (1977).
[36] G.D. Gilliland, A. Antonelli, D.J. Wolford, K.K. Bajaj, J. Klem, J.A. Bradley, Phys. Rev. Lett. 71 (1993) 3717.
[37] A.B. Dzyubenko, G.E.W. Bauer, Phys. Rev. B 51 (1995) 14524.
[38] J. Feldmann, G. Peter, E.O. Göbel, P. Dawson, K. Moore, C. Foxon, R.J. Elliott, Phys. Rev. Lett. 59 (1987) 2337.
[39] B.L. Altshuler, P.A. Lee, R.A. Webb, in: V.M. Agranovich, A.A. Maradudin (Eds.), Mesoscopic Phenomena in Solids, North-Holland, Amsterdam, 1991.
[40] L.V. Butov, A.L. Ivanov, A. Imamoglu, P.B. Littlewood, A.A. Shashkin, V.T. Dolgopolov, K.L. Campman, A.C. Gossard, Phys. Rev. Lett. 86 (2001) 5608.
[41] L.V. Butov, C.W. Lai, D.S. Chemla, Yu.E. Lozovik, K.L. Campman, A.C. Gossard, Phys. Rev. Lett. 87 (2001) 216804.
[42] L.V. Butov, A.C. Gossard, D.S. Chemla, cond-mat/0204482 L.V.Butov, A.C.Gossard, D.S. Chemla Nature 418 (2002) 751.
[43] D. Snoke, S. Denev, Y. Liu, L. Pfeiffer, K. West, Nature 418 (2002) 754.
[44] K.E. Strecker, G.B. Partridge, A.G. Truscott, R.G. Hulet, Nature 417 (2002) 150.
[45] G.I. Taylor, Philos. Trans. R. Soc. London Ser. A 223 (1923) 289.
[46] L.V. Keldysh, Contemp. Phys. 27 (1986) 395.
[47] S. Chandrasekhar, E. Fermi, ApJ 118 (1953) 116.
[48] D. O'Dell, S. Giovanazzi, G. Kurizki, V.M. Akulin, Phys. Rev. Lett. 84 (2000) 5687.
[49] S. Giovanazzi, G. Kurizki, I.E. Mazets, S. Stringari, Europhys. Lett. 56 (2001) 1.